Design and Testing of a Thermobaric Piercing Projectile for 73 mm Recoilless Canon

Ovidiu IORGA, Tudor V. ȚIGĂNESCU, Alexandru MARIN,
Mihail MUNTEANU, and Ionuț SIMION

***Abstract* —Urban area combat theaters require the use of portable weapons capable to neutralize targets inside buildings or light armored improvised vehicles. This work presents the design and testing of piercing ammunition for 73 mm recoilless canon with fragmentation and thermobaric effect. The advantages relative to its intended use are represented by its capability to pierce reinforced concrete and light armored targets, the fragmentation and thermobaric explosive delayed effect, capable to neutralize both soft targets and structures, and the reduced mass and dimensions of the armament system intended to be used. The warhead is composed of a piercing projectile with thin wall in order to accommodate an explosive charge with thermobaric effect, initiated by a bottom fuse. The warhead is coupled with a rocket motor in order to augment the initial velocity of the projectile for the maximization of the piercing capability. The paper presents the process of forging and machining of the warhead shell as well as the numerical simulation regarding the terminal ballistics of the ammunition, which was validated trough live fire experiments.**

***Index Terms*—Forging, piercing, recoilless, terminal ballistics, thermobaric.**

I. Introduction

Nowadays, there are multiple studies conducted on the potential to improve protective materials, such as adding fibers to concrete or using multi-layer composites for vehicle body. On the other hand, there are also studies focused on improving material properties employed to manufacture different types of ammunition, which can be used to penetrate armor [4].

Piercing projectiles are a special kind of ammunition, which is designed to penetrate through hard targets like alloyed steel for armor structures. In addition, due to the high yield strength of materials, such projectiles are also capable of piercing concrete structures.

In terms of manufacturing process, piercing ammunition used during tests was made of forged structural alloy steel; on which several heat treatments were applied [1].

The samples were submitted to follow up heat treatments in order to obtain specific mechanical properties, such as yield stress resistance, tensile strength, hardness, percent elongation, etc.

II. Design of the Ammunition

The ammunition is composed of a piercing projectile obtained by forging, machining and hardening of 35 HGSA rectangular bars. In its design, the ogive has a sharp tip in order to displace the fractured concrete target. The ogive is made of thick steel. The geometry progressively thins up to the walls in order to accommodate 400 cm^3 of explosive charge. The bottom part of the shell is designed to accommodate the delayed fuse and to connect with the rocket motor. The rocket motor has an under-caliber circumference, is made of steel and is loaded with 500 g of double base propellant single grain, with constant burning geometry. It is ignited by an inertial system and has a delay ranging between 0.025 s and 0.050 s in order to start at 10–15 m away from the muzzle. The burn time for the motor is between 0.300 s and 0.500 s, depending on the ambient temperature. The ammunition is expelled from the muzzle by a lamellar geometry propellant charge assimilated from the PG-9 ammunition. In Fig. 1, the main components of the ammunition are presented, while, in Table I, there are some constructional and performance parameters presented.

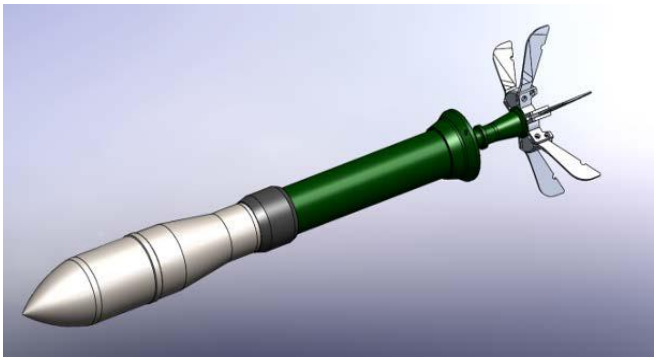

Figure 1. The warhead and the rocket motor of the ammunition, on the trajectory (without propellant charge and with opened stabilizing fins)

This work was supported by a grant of the Romanian Ministry of Education and Research, CCCDI – UEFISCDI, project number PN-III-P2-2.1-PTE-2019-0256, within PNCDI III.

O. IORGA is chemical engineer and PhD candidate within the Doctoral School of Military Technical Academy "Ferdinand I" in Bucharest in the field of mechanical engineering. Currently he is researcher at Scientific Research Center for CBRN Defense and Ecology, in Bucharest, Romania (email: ovidiu.iorga@nbce.ro).

T. V. ȚIGĂNESCU is professor at Military Technical Academy "Ferdinand I" in Bucharest and general director of the Military Equipment and Technologies Research Agency from Clinceni, Romania (email: viorel.tiganescu@mta.ro)

A. MARIN is junior scientific researcher at Scientific Research Center for CBRN Defense and Ecology, Bucharest, Romania and PhD candidate at Military Technical Academy "Ferdinand I" in Bucharest (email: alexandru.marin@nbce.ro).

M. MUNTEANU is junior scientific researcher at Scientific Research Center for CBRN Defense and Ecology, Bucharest, Romania and PhD candidate at Military Technical Academy "Ferdinand I" in Bucharest (email: mihail.munteanu@nbce.ro).

I. SIMION is mechanical engineer. He currently holds the position of design process engineer at UM Plopeni factory in Prahova County, Romania (email: ionut.simion09@yahoo.com).

TABLE I. THE AMMUNITION'S MAIN CHARACTERISTICS

Parameter	Value
Mass (without propellant charge)	5.4 kg
Mass of the warhead	3700 g
Mass of the explosive charge	780 g
Length of the warhead	300 mm
Caliber	73 mm
Initial velocity	270±5 m/s
Maximum velocity	450±10 m/s
Maximum range	1200 m
Aiming range	800 m
Piercing capacity (in C35/C37 double reinforced concrete)	>200 mm
Piercing capacity (in homogenous armor)	>20 mm

III. MANUFACTURING PROCESS OF PROJECTILE

The manufacturing process of the projectile consists in a sequence of mechanical and metallurgical phases with intermediary and final verifications.

Each metallic constituent part of the projectile is submitted to a Total Quality Control (TQC) phase before being sent to the pyrotechnic department. After setting up the explosive charge, the final product is tested within a firing range. The main operations of the manufacturing process are depicted in Fig. 2.

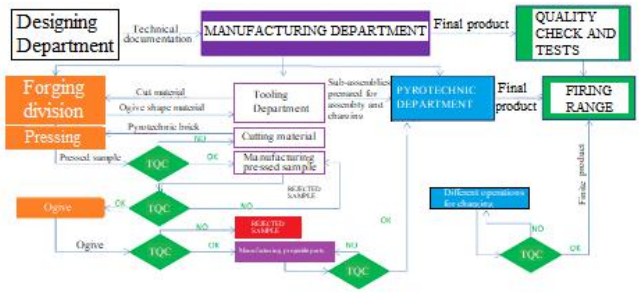

Figure 2. Schematic manufacturing process of the projectile

The manufacturing process of the projectile consists in forging operations performed on a rectangular bar, as shown in Fig. 3. The plastic deformation occurs above their recrystallization temperature, in order to allow material to retain shape after cooling. Therefore, the heating process takes places at a constant temperature of 820°C, for both raw material and following ogive part of the projectile.

Subsequent phases include lathe cutting for projectile body, ogive part, shell, cap, fuse, etc.

Figure 3. Different phases in the manufacturing process of projectile

The heat treatment applied for improved mechanical properties is a follow-up to the machining process of the projectile [7].

Steps of technological process include:

1. Display the 50 moulded pieces in refractory steel baskets (of 1000×1000×200 mm dimension) used for annealing. Each metal part is separated from the other in order to ensure a minimum distance of 50 mm.

2. The basket containing moulded parts was introduced into the furnace at a temperature of $T = 600°C \pm 10°C$;

3. The metal was held at temperature $T = 600°C \pm 10°C$, for about 60 min;

4. Transfer the basket containing metal parts into another furnace previously heated to 850°C;

5. Heat the metal parts with a heating speed of 150–200°C/h until the parts reach the temperature within the furnace of 850°C;

6. Maintain parts at 850°C for 40 minutes;

7. Remove parts from furnace and allow a slow air cooling until it reaches the surrounding temperature;

8. Record technological parameters specific to the annealing process, and the heat treatment diagram into a data register.

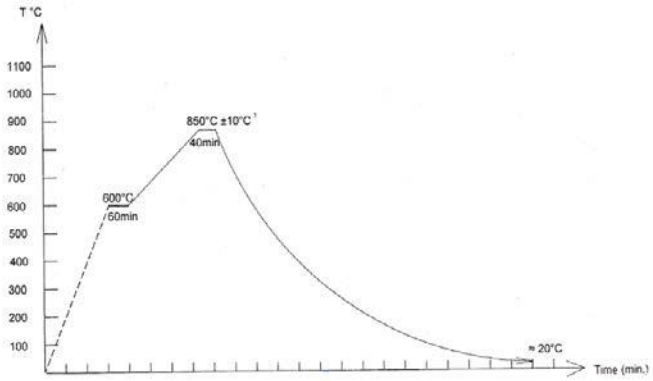

Figure 4. Thermal treatment diagram of 35HGSA hardened steel

Steps of final heat treatment include:

1. Display the 50 moulded pieces in 2 refractory steel baskets (25 pieces in one basket and 25 pieces in second basket). Each basket will contain parts belonging to the same batch. Also, each metal part will be positioned with the tip downwards, in vertical position;
2. The two baskets containing moulded parts will be submitted to an intermittent Martempering;
3. First step, pre-heating, is performed in 2 phases (heating up to 400°C, held for 60 min, and heating up to 700°C, held for another 60 min;
4. Second step consists in heating up to an austenite crystalline structure, at 815°C, and held for 30 min. The furnace was preheated to 900°C;
5. After performing a Martempering, the cooling is made with water, for minimum 20 min;
6. After hardening process, there will be performed a Brinell test for each piece, within a time range of 4 hours after the heat treatment;
7. Parts with lower hardness than the specified value will be rejected, and parts with higher hardness will be submitted to an additional tempering (at 250°C, for 2 hours, in the air), in order to decrease hardness.

 Digital Object Identifier 10.32754/JMT.2020.2.04

The diagram depicting the steps of final treatment is presented in Fig. 5.

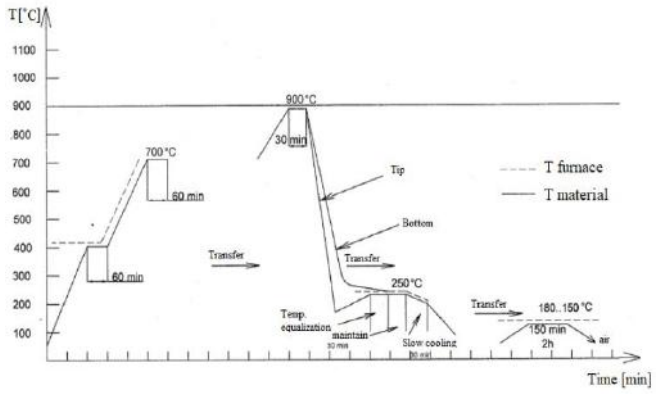

Figure 5. Final thermal treatment diagram of 35HGSA hardened steel

IV. Numerical Simulation

The numerical simulation of the impact between the steel/reinforced concrete targets was made using Ansys software [2, 3]. The explicit analysis was configured with Ansys workbench coupled with Ansys Autodyn processor.

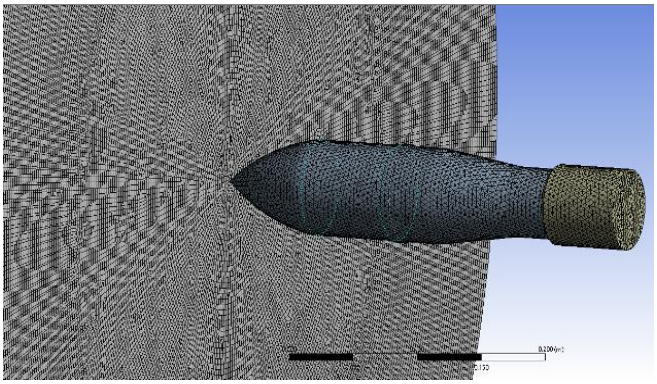

Figure 6. Model meshing of the impact between the projectile and 20 mm homogenous steel target.

In Fig. 6, the model for both target and projectile, after applying mesh, is presented. A linear, and not a parabolic meshing, was used, of size 0.004 m, resulting in a number of 393,833 nodes and 424,030 elements, adequate for observing deformation due to impact. Choosing a mesh with smaller size would have led to an increase in computational time.

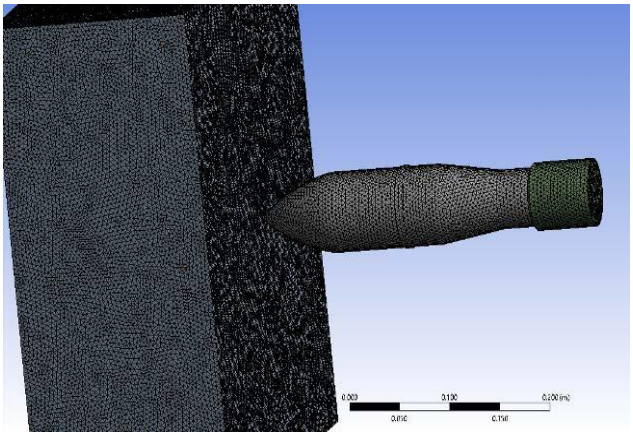

Figure 7. Model meshing of the impact between the projectile and 200 mm C35/C37 concrete double reinforced with rebar.

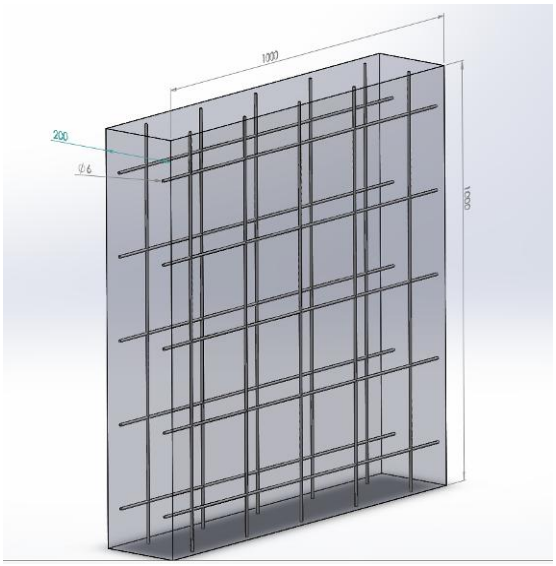

Figure 8. Detail on the model for 200 mm thick concrete target reinforced with 6 mm steel rebars

Similar to the previous simulation, in this case a linear meshing was also used for the 200 mm plate. The mesh size was 0.004 m, resulting in a total number of 1,236,635 nodes and 1,311,454 elements.

Initial conditions for the simulation:

- initial velocity of the projectile: 500 m/s;
- the targets: reinforced concrete and homogenous steel had fixed support on outside faces.

Regarding the parameters for both target and ammunition, within the simulation materials with properties depicted in Appendix A were used.

V. Results of Simulation

A. Between armor steel and projectile

The tip of the ogival part was eroded and deformed, but with no consequences on the structural integrity. No plastic deformation of the projectile body was observed.

As it was to be expected, after impact, the plate submitted to tests has absorbed a part of the impact energy (due to its deformation), which led to a decrease of the kinetic energy of projectile by approximately 19%.

At the same time, after perforating the target, projectile speed decreased with a rough estimate of 50 m/s (10%).

According to simulation, as opposed to the concrete plate, the armor steel was perforated, but without many material detachment.

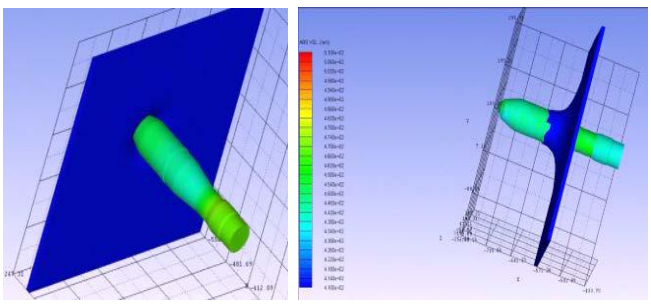

Figure 9. Numerical simulation of the impact between the projectile and the armor plate

B. Between concrete structure and projectile

The tip of the ogival part was eroded because of the fact that geometrical strain erosion was set to a ratio of 1.5. The rest of the shell body suffered only transient elastic deformation without affecting the explosive charge or the integrity of the warhead [5]. The projectile velocity decreased after target penetration with 143 m/s (by 28.6%) while the kinetic energy decreased by 49%.

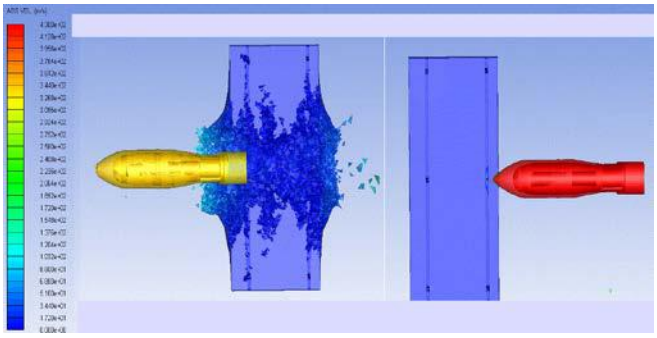

Figure 10. Numerical simulation of the impact between the projectile and the concrete target

Comparing the two simulations, it can be observed that the concrete plate absorbed a higher percent of projectile kinetic energy as opposed to the steel plate, which is reflected in a considerable decrease of projectile speed after perforation.

On the other hand, the last simulation showed that material detachments can also be observed, which may lead to human injuries or deaths, as well as material damage.

VI. Field Tests

Live fires have been conducted using ammunition with mockup explosive charge and fuse. The distance between the muzzle and the target was set at 200 m in order for the projectile to acquire maximum velocity, with the aid of the rocket motor, before impact. The impact angle was set perpendicular on the direction of the projectile [6, 8].

The targets consisted of a 20 mm thick armor plate (standard material for ballistic testing) and a double reinforced C37/C37 concrete block with 1 m × 2 m × 0.2 m dimensions. A fast camera was used to capture the impact, model Photron Fastcam SA 1.1 set at 5400 fps and 1/12000 shutter speed. Trigger was set to sound at a pre-trigger acquisition of 30%.

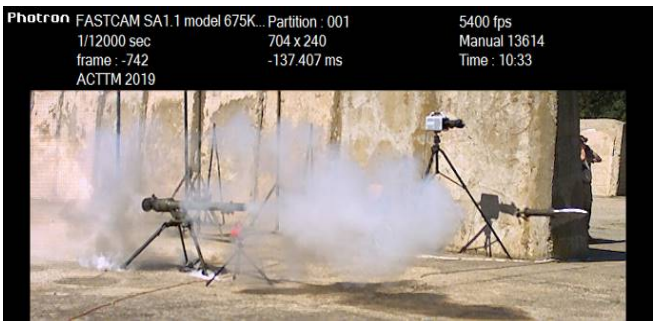

Figure 11. Live firing of the piercing ammunition with thermobaric effect

Figure 12. Concrete target penetration tests

Figure 13. Homogenous steel armor penetration tests

Figure 14. The ammunition before firing and after steel target penetration tests

VII. Conclusion

This fabrication process for the shell is properly carried out in respect with the obtained results. The dimensional and axial symmetry of the projectile has been evaluated. The numerical simulation revealed that no residual deformation will be present on the projectile after the impact, neither on the selected targets, without considering the erosion of the tip of the shell, in order to reduce the calculation time of the numerical simulation.

Field trials validated both the numerical simulation and the design and fabrication process for the projectile. Further work will be carried out in order to determine the maximum piercing capabilities of the projectile and the residual velocity, determined with appropriate equipment.

 Digital Object Identifier 10.32754/JMT.2020.2.04

APPENDIX A

TABLE II. PROPERTIES OF STEEL TARGET-STEEL 4340

Equation of State	**Linear**
Reference density	7.83000E+00 (g/cm^3)
Bulk Modulus	1.59000E+08 (kPa)
Reference Temperature	2.95150E+02 (K)
Specific Heat	4.77000E+02 (J/kgK)
Thermal Conductivity	0.00000E+00 (J/mKs)
Strength	Johnson Cook
Shear Modulus	8.18000E+07 (kPa)
Yield Stress	7.92000E+05 (kPa)
Hardening Constant	5.10000E+05 (kPa)
Hardening Exponent	2.60000E-01 (none)
Strain Rate Constant	1.40000E-02 (none)
Thermal Softening Exponent	1.03000E+00 (none)
Melting Temperature	1.79300E+03 (K)
Ref. Strain Rate (/s)	1.00000E+00 (none)
Strain Rate Correction	1st Order
Maximum Expansion	1.00000E-01 (none)
Minimum Density Factor	1.00000E-04 (none)
Minimum Density Factor (SPH)	2.00000E-01 (none)
Maximum Density Factor (SPH)	3.00000E+00 (none)
Minimum Soundspeed	1.00000E-06 (m/s)
Maximum Soundspeed (SPH)	1.01000E+20 (m/s)
Maximum Temperature	1.01000E+20 (K)

TABLE III. PROPERTIES OF EXPLOSIVE CHARGE-POLYCARBONATE

Equation of State	Shock
Reference density	1.20000E+00 (g/cm^3)
Gruneisen coefficient	6.10000E-01 (none)
Param. C1	1.93300E+03 (m/s)
Param. C2	2.35000E+03 (m/s)
Param. S1	2.65000E+00
Param. S2	1.60000E+00
Parameter Quadratic S2	0.00000E+00 (s/m)
Relative volume, VE/V0	7.01000E-01 (none)
Relative volume, VB/V0	7.42000E-01 (none)
Reference Temperature	2.95150E+02 (K)
Specific Heat	0.00000E+00 (J/kgK)
Thermal Conductivity	0.00000E+00 (J/mKs)
Strength	Multilinear Hardening
Shear Modulus	1.00000E+06 (kPa)
Eff. Plastic Strain #1	0.00000E+00,
Eff. Plastic Strain #2	1.00000E-01
Eff. Plastic Strain #3	5.00000E-01
Eff. Plastic Strain #4	6.00000E-01
Eff. Plastic Strain #5	7.00000E-01
Stress #1/	8.06000E+04 (kPa)
Stress #2	8.80000E+04 (kPa)
Stress #3	1.42500E+05 (kPa)
Stress #4	1.68000E+05 (kPa)
Stress #5	1.87000E+05 (kPa)
Hardening	Isotropic
Failure	Plastic Strain
Plastic Strain	1.00000E+20 (none)
Crack Softening	No
Stochastic failure	No
Erosion	None
Maximum Expansion	1.00000E-01 (none)
Minimum Density Factor	1.00000E-04 (none)
Minimum Density Factor (SPH)	2.00000E-01 (none)
Maximum Density Factor (SPH)	3.00000E+00 (none)
Minimum Soundspeed	1.00000E-06 (m/s)
Maximum Soundspeed (SPH)	1.01000E+20 (m/s)
Maximum Temperature	1.01000E+20 (K)
Reference:	-

TABLE IV. PROPERTIES OF AUXILIARY PROJECTILE ELEMENTS AND BOTTOM FUSE – ALLUMINIUM 6061 – T6

quation of State	**Shock**
Reference density	2.70300E+00 (g/cm^3)
Gruneisen coefficient	1.97000E+00 (none)
Parameter C1	5.24000E+03 (m/s)
Parameter S1	1.40000E+00 (none)
Reference Temperature	2.95150E+02 (K)
Specific Heat	8.85000E+02 (J/kgK)
Thermal Conductivity	0.00000E+00 (J/mKs)
Strength	**Steinberg Guinan**
Shear Modulus	2.76000E+07 (kPa)
Yield Stress	2.90000E+05 (kPa)
Maximum Yield Stress	6.80000E+05 (kPa)
Hardening Constant	1.25000E+02 (none)
Hardening Exponent	1.00000E-01 (none)
Derivative dG/dP	1.80000E+00 (none)
Derivative dG/dT	-1.70000E+04 (kPa/K)
Derivative dY/dP	1.89080E-02 (none)
Melting Temperature	1.22000E+03 (K)
Maximum Expansion	1.00000E-01 (none)
Minimum Density Factor	1.00000E-04 (none)
Minimum Density Factor (SPH)	2.00000E-01 (none)
Maximum Density Factor (SPH)	3.00000E+00 (none)
Minimum Soundspeed	1.00000E-06 (m/s)
Maximum Soundspeed (SPH)	1.01000E+20 (m/s)
Maximum Temperature	1.01000E+20 (K)

TABLE V. PROPERTIES FOR THE SHELL OF THE PROJECTILE: 35HGSA

Equation of State	Linear
Reference density	7.83000E+00 (g/cm^3)
Bulk Modulus	1.59000E+08 (kPa)
Reference Temperature	2.95150E+02 (K)
Specific Heat	4.77000E+02 (J/kgK)
Thermal Conductivity	0.00000E+00 (J/mKs)
Strength	Johnson Cook
Shear Modulus	8.18000E+07 (kPa)
Yield Stress	1.28000E+06 (kPa)
Hardening Constant	5.10000E+05 (kPa)
Hardening Exponent	2.60000E-01 (none)
Strain Rate Constant	1.40000E-02 (none)
Thermal Softening Exponent	1.03000E+00 (none)

Melting Temperature	1.79300E+03 (K)
Ref. Strain Rate (/s)	1.00000E+00 (none)
Strain Rate Correction	1st Order
Maximum Expansion	1.00000E-01 (none)
Minimum Density Factor	1.00000E-04 (none)
Minimum Density Factor (SPH)	2.00000E-01 (none)
Maximum Density Factor (SPH)	3.00000E+00 (none)
Minimum Soundspeed	1.00000E-06 (m/s)
Maximum Soundspeed (SPH)	1.01000E+20 (m/s)
Maximum Temperature	1.01000E+20 (K)

TABLE VI. PROPERTIES OF REBARS-STEEL 1006

Equation of State	**Shock**
Reference density	7.89600E+00 (g/cm^3)
Gruneisen coefficient	2.17000E+00 (none)
Parameter C1	4.56900E+03 (m/s)
Parameter S1	1.49000E+00 (none)
Parameter Quadratic S2	0.00000E+00 (s/m)
Parameter C2	0.00000E+00 (m/s)
Parameter S2	0.00000E+00 (none)
Reference Temperature	2.95150E+02 (K)
Specific Heat	4.52000E+02 (J/kgK)
Thermal Conductivity	0.00000E+00 (J/mKs)
Strength	**Johnson Cook**
Shear Modulus	8.18000E+07 (kPa)
Yield Stress	3.50000E+05 (kPa)
Hardening Constant	2.75000E+05 (kPa)
Hardening Exponent	3.60000E-01 (none)
Strain Rate Constant	2.20000E-02 (none)
Thermal Softening Exponent	1.00000E+00 (none)
Melting Temperature	1.81100E+03 (K)
Ref. Strain Rate (/s)	1.00000E+00 (none)
Strain Rate Correction	1st Order
Maximum Expansion	1.00000E-01 (none)
Minimum Density Factor	1.00000E-04 (none)
Minimum Density Factor (SPH)	2.00000E-01 (none)
Maximum Density Factor (SPH)	3.00000E+00 (none)
Minimum Soundspeed	1.00000E-06 (m/s)
Maximum Soundspeed (SPH)	1.01000E+20 (m/s)
Maximum Temperature	1.01000E+20 (K)

ACKNOWLEDGMENT

The authors would like to thank senior researcher Constantin Puica, from Military Equipment and Technologies Research Agency for providing support in the numerical simulation, including the software and hardware resources.

REFERENCES

[1] A. V. Kirichek *et al.*, "The investigation of the deformation wave hardening effect on the strength of the medium and low alloy steels" *IOP Conf. Ser.: Mater. Sci. Eng.*, vol. 177, 2017. doi:10.1088/1757-899X/177/1/012121

[2] D. Burger *et al.*, "Ballistic impact simulation of an armour-piercing projectile on hybrid ceramic/fiber reinforced composite armours", *International Journal of Impact Engineering*, vol. 43, pp. 63-77, 2012. doi:10.1016/j.ijimpeng.2011.12.001

[3] J. Bernetic *et al.*, "Phenomena in penetrating piercing bullets in armored steel plate", *Metalugija*, vol. 55, pp. 95-98, 2016.

[4] J. Feng *et al.*, "An armour-piercing projectile penetration in a double-layered target of ultra-high-performance fiber reinforced concrete and armour steel: experimental and numerical analyses", *Materials and Design*, 2016. doi:10.1016/j.matdes.2016.04.021

[5] K. G. Rakvag *et al.*, "An experimental study on the deformation and fracture modes of steel projectiles during impact", *Materials and Design*, pp. 242-256, 2013. doi.org/10.1016/j.matdes.2013.04.036

[6] M. A. Iqbal *et al.*, "An investigation of the constitutive behavior of Armox 500T steel and armor piercing incendiary projectile material", *International Journal of Impact Engineering*, pp. 146-164, 2016.

[7] R. Stoica *et al.*, "Considerations regarding the comparative determination of materials hardness submitted to heat treatments" *Ingineria automobilului*, nr. 54, pp. 18-20, 2020.

[8] S. H. Atapek and S. Karagoz, "Ballistic impact behavior of a tempered bainitic steel against 7.62 mm armour piercing projectile", *Defence Science Journal*, vol. 61, Jan. 2011. doi:10.14429/dsj.61.411